Indirect methods to control population distribution in a large spin system

2017 New J. Phys. 19 033016

(http://iopscience.iop.org/1367-2630/19/3/033016)

New Journal of Physics
The open access journal at the forefront of physics

Deutsche Physikalische Gesellschaft DPG
IOP Institute of Physics

Published in partnership with: Deutsche Physikalische Gesellschaft and the Institute of Physics

OPEN ACCESS

RECEIVED
19 December 2016

REVISED
3 February 2017

ACCEPTED FOR PUBLICATION
10 February 2017

PUBLISHED
10 March 2017

PAPER

Indirect methods to control population distribution in a large spin system

Lingfei Zhao[1], **Maxim Goryachev**[2,3], **Jeremy Bourhill**[2] **and Michael E Tobar**[2]

[1] Department of Physics, Nanjing University, Nanjing 210093, People's Republic of China
[2] ARC Centre of Excellence for Engineered Quantum Systems, University of Western Australia, 35 Stirling Highway, Crawley WA 6009, Australia
[3] Author to whom any correspondence should be addressed.

E-mail: maxim.goryachev@uwa.edu.au **and** michael.tobar@uwa.edu.au

Keywords: spins in solids, large spin system, whispering gallery mode, Landau–Zener transition

Abstract

We demonstrate how a large spin system ($S = 7/2$) with the ground and first excited state separated by a seven-photon transition exhibits nonequilibrium thermodynamic properties and how the population distribution may be manipulated using coupling between energy levels. The first method involves non-adiabatic passage through an avoided level crossing controlled with an external DC magnetic field and the resulting Landau–Zener transition. The second method is based on external cavity pumping to a higher energy state hybridised with another state that is two single-photon transitions away from the ground state. The results are confirmed experimentally with a Gd^{3+} impurity ion ensemble in a YVO_4 crystal cooled to 20 mK, which also acts as a microwave photonic whispering gallery mode resonator. Extremely long lifetimes are observed due to the large number of photons required for the transition between the ground and first excited states.

1. Introduction

Physical systems based on the light–matter interaction in general and quantum electrodynamics (QED) with 'spins-in-solid' in particular have found a very broad range of applications. They constitute a platform for lasers [1], masers [2, 3], quantum information processing units [4, 5], communication devices [6, 7], clocks [8, 9], sensors [10], as well as probes in fundamental physics [11, 12]. Particular interest is devoted to rare-earth spin ensembles in crystals due to their long lifetimes [13–15]. Although many aspects of such systems have been investigated in detail, many other features are yet to be discovered. Such new peculiarities not only give birth to new generations of existing devices and tools but also open avenues for new applications.

In this work, we experimentally demonstrate a new configuration spin system that can bring new ideas to the field of quantum electrodynamics with spins. In particular, we consider an unusual manifestation of the spin angular momentum conservation law appearing through unusual population dynamics in a multilevel spin system. Although it is well understood that light–matter interaction for small-enough coupling (not reaching the ultra-strong coupling regime, i.e., when coupling is small enough compared to the resonance frequencies involved) is a subject of conservation of energy and momentum, the role of the latter is not usually discussed though it may play a very crucial role in many systems. The spin angular momentum conservation law imposes an additional selection rule for spin–photon interaction by creating photons with circular polarisation and thus the spin angular momentum. For instance, it shapes the system response for a photon interacting with a spin ensemble in a whispering gallery mode (WGM) cavity by breaking the time-reversal symmetry [16, 17]. The quantum system configuration in such systems may be significantly different from that of traditional QED systems, giving new properties that can be exploited for existing and emerging applications.

A typical setup implementing spin–photon interaction consists of a cavity coupled to a two-level system (TLS) or an ensemble of TLS [2, 18–21]. Each TLS may absorb or emit one photon by transiting between the excited and ground states. In this case, these states are separated by spin number one ($\Delta m = 1$). On the other

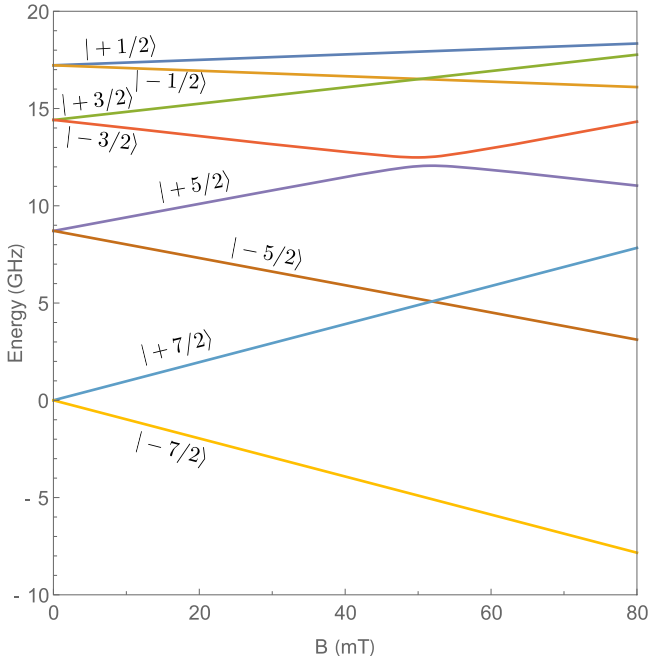

Figure 1. Energy levels of Gd^{3+} in YVO_4 as a function of magnetic field B parallel to the crystal c-axis.

hand, the ground and the first excited states may be separated by more than one spin number ($\Delta m > 1$). In this case, the transition requires the corresponding number of photons to conserve the spin number, making the transition less probable as Δm photons are simultaneously required to interact with a spin. This fact not only reduces spin–cavity coupling but also spin interaction with the environment. As a result, spins excited to the first excited states exhibit significantly lower decay rate. On the other hand, despite lower coupling to the cavity, the spin state can be manipulated via coupling to other excited states. This work demonstrates the possibility of manipulation of such a system via cavity pumping to higher excited states and the Landau–Zener effect in a 'spins-in-solid' experimental setup.

2. Gd^{3+}: YVO_4 spin system

The multi-photon transition spin system is realised with the Gd^{3+} impurity ion ensemble in YVO_4 crystal having the zircon structure [22]. This impurity is a $7/2$ spin system, with eight energy levels controllable by an external magnetic field via Zeeman splitting [23]. At zero field, the energy structure consists of four degenerate pairs of levels in the microwave frequency range (figure 1) [24, 25]. The most important feature of such a system is that the two lowest energy levels are the $|-7/2\rangle$ and $|+7/2\rangle$ spin states ($\Delta m = 7$), requiring seven photons for a transition. It is this large spin number difference that is exploited in this work to lock the spin system in the first excited state ($|+7/2\rangle$ state). The $|-7/2\rangle$ state plays the role of the ground state throughout this work.

The other important feature of the Gd^{3+}:YVO_4 spin system is finite coupling between different energy levels. The origins of this coupling can vary from imperfections of the crystal structure to imperfect alignment of the external field with respect to the c-axis. This coupling is exploited for spin transfer between states with different spin number with respect to the ground state.

In the following theoretical and experimental sections, we limit the discussion to the case of the lowest temperature routinely achievable with dilution refrigerators $T = 20$ mK. This temperature is low enough to keep the whole spin ensemble at the lowest energy state in thermal equilibrium.

2.1. Preparing a nonequilibrium state

At zero magnetic field and for temperatures approaching absolute zero, the population of the Gd^{3+} spin ensemble condenses to the degenerate $|\pm 7/2\rangle$ states at the thermal equilibrium. This means that the spin ensemble has an equal distribution between these states. For nonzero magnetic fields, the thermal equilibrium deviates from this 50%–50% distribution, approaching complete 100% occupation of the ground state. For a normal $\Delta m = 1$ spin system, this thermalisation would happen naturally on the time scale corresponding to the strength of coupling to the environment. For the seven-photon transition, however, half of the population is naturally locked at the $|+7/2\rangle$ state and cannot be easily thermalised. Thus, the overall system exists in a non-

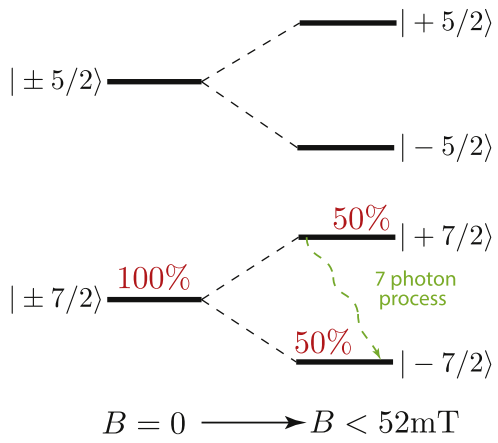

Figure 2. Generation of the equally distributed state and the seven-photon process. Only $|\pm 7/2\rangle$ and $|\pm 5/2\rangle$ are shown. Percentages show the corresponding level occupancy.

thermal equilibrium state with equal distribution, as the external magnetic field is initially slowly detuned from zero. This situation is bounded from the top at $B = 52$ mT, where energy level $|+7/2\rangle$ and $|-5/2\rangle$ come to close proximity with one another. The overall process is shown in figure 2.

Occupancy of the $|\pm 7/2\rangle$ states may be verified by measuring the coupling strength between a cavity mode and spin transitions from the corresponding states to some higher-energy states. Indeed, the effective coupling strength for a $|n/2\rangle$ state is $g_{\text{eff}} = g_0\sqrt{N_{|n/2\rangle}}$, where g_0 is the coupling strength of an individual spin and $N_{|n/2\rangle}$ is the number of spins in the corresponding state under the given experimental conditions. g_0 is determined by spin properties together with the other parameters such as cavity mode filling factors [26, 27]:

$$g_0 = \frac{g_d\,\mu_B}{2h}\sqrt{\frac{hf_0\mu\beta}{2V}}, \tag{1}$$

where g_d is the Landé g-factor, μ_B is Bohr magneton, h is Planck constant, f_0 is the frequency of the cavity mode, μ is the permeability of the crystal, β is the magnetic field filling factor of the cavity mode (which can be calculated by finite element analysis), and V is the volume of the crystal.

2.2. Landau–Zener assisted thermalisation

The energy diagram of a Gd^{3+} ion in YVO_4 suggests that, for the external magnetic field near 52 mT energy levels, $|+7/2\rangle$ and $|-5/2\rangle$ cross one another. This picture holds true only for an ideal crystal with external field exactly parallel to the crystal c-axis. In a real experiment this is not the case, and small misalignments between these directions cause coupling g_{LZ} between the $|+7/2\rangle$ and $|-5/2\rangle$ energy levels. As a result of this coupling, the levels never cross and form an avoided level crossing (ALC), with the whole system tunable via the external B-field.

In the situation where energy levels are coupled and the external control parameter is tuned across the ALC, a quantum system exhibits quantum tunnelling Landau–Zener (LZ) transition [28, 29]. In the discussed system, the tunnelling occurs from the populated $|+7/2\rangle$ state to the empty $|-5/2\rangle$. The latter is only a single-photon transition away from the lowest energy state $|-7/2\rangle$. As a result, the relaxation to this state occurs on the time scale of the system relaxation time. Consequently, the whole population of $|-5/2\rangle$, i.e., 50% of the total ensemble (see right situation in figure 3), relaxes back to the ground $|-7/2\rangle$ state, forming the thermal equilibrium state via the LZ transition. This process occurs when the control parameter is tuned across 52 mT (middle situation in figure 3). Thus, the seven-photon population, which has 50% of the spins locked at the first excited stated, is overcome by the non-adiabatic crossing of energy levels, and a normal one-photon relaxation occurs requiring no external pumping field.

The Landau–Zener assisted thermalisation may be detected by measuring the coupling between a cavity mode and the spin transitions from both the $|+7/2\rangle$ and $|-7/2\rangle$ levels to $|+5/2\rangle$ and $|-5/2\rangle$, respectively. Before the event, the population will be equally split between the two lowest levels, and afterwards all ions will be in the ground state, as depicted in figure 3. Real-time observation of this effect is not possible in our cavity implementation, as there does not exist a cavity mode of frequency equivalent to the transition energy at $B = 52$ mT.

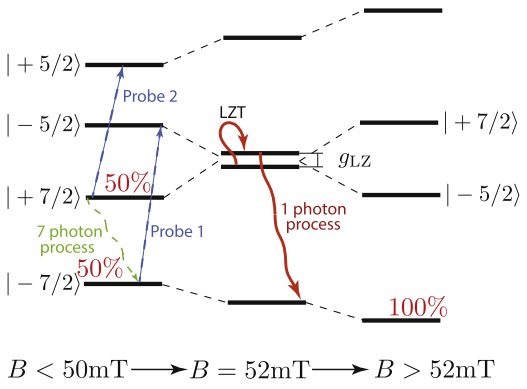

Figure 3. Ensemble thermalisation through the Landau–Zener effect. Only four lower energy levels are shown.

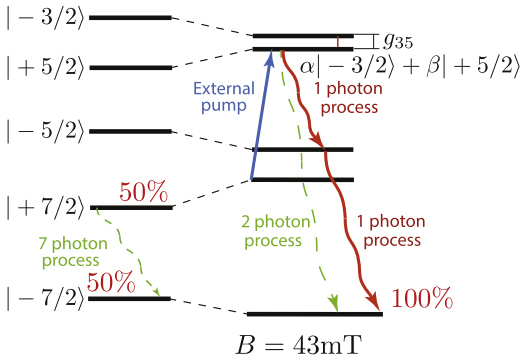

Figure 4. Cavity-assisted thermalisation via pumping to hybridised $\alpha|+5/2\rangle + \beta|-3/2\rangle$ state and decay to the ground state through $|-5/2\rangle$.

2.3. Cavity-driven thermalisation

In addition to the Landau–Zener mechanism, the population can be transferred via an external pump field. In fact, one can pump the population at the $|+7/2\rangle$ state in figure 2 (final situation) to a higher-energy state that is closer to the ground state in number of photons required for relaxation. For the case of Gd^{3+} in YVO_4, the procedure may be implemented as follows: the population from the $|+7/2\rangle$ state is pumped to the $|+5/2\rangle$ (one-photon efficient process), which is hybridised with $|-3/2\rangle$ at $B = 43$ mT, and ions at the $|-3/2\rangle$ state decay to $|-7/2\rangle$ via $|-5/2\rangle$ (two single-photon processes). The energy level diagram for the cavity-driven thermalisation is shown in figure 4. The coupling between the $|+5/2\rangle$ and $|-3/2\rangle$ states arises due to the fourthfold symmetry of the crystal and may exceed 100 MHz [24]. At the working 43 mT, the hybridised state is $0.05|-3/2\rangle + 0.95|+5/2\rangle$, which together with the splitting of the decay into two single-photon processes may decrease the efficiency of the thermalisation. On the other hand, the overall process efficiency may be controlled via the strength of the external pump. Indeed, the time required to excite all the spins from $|+7/2\rangle$ to the hybridised higher-energy state depends on the spin–photon coupling and the number of cavity photons.

Cavity-driven thermalisation may be observed in real time, as it does not require any tuning parameters to be involved. For this purpose, one can monitor the cavity transmission when it is tuned on the $|+7/2\rangle$ to $\alpha|-3/2\rangle + \beta|+5/2\rangle$ at $B = 42$ mT, as it is a function of g_{eff}.

3. Experimental realisation

To observe the effects described in the previous section, the 'spins-in-solids' approach [19, 30, 31] with a WGM system [32] is implemented. The system utilises a single cylindrical YVO_4 crystal both as a cavity and ion host. This ensures the highest filling and quality factors. The YVO_4 crystal has a diameter of 13.9 mm and height of 14.3 mm, which provides several WGMs in the 5–20 GHz frequency range. The spin–photon interaction is maximised for WGMs with radial (or transverse) component of the magnetic field (WGH modes). The crystal is confined inside an oxygen-free copper cavity and cooled to 20 mK inside a dry dilution refrigerator system. A superconducting magnet is used to provide a DC magnetic field almost parallel to the crystal *c*-axis. The external

pump and probe fields are provided by a network analyser connected to the cavity via electric field probes through a chain of cold attenuation (40 dB in total). The transmitted signal is detected via a 4 K low-noise (high-electron-mobility transistor) HEMT amplifier providing the cavity transmission coefficient S_{21}. The experimental setup is explained in detail in previous experiments [16, 17, 26].

The cavity transmission S_{21} is related to the coupling strength between the spin ensemble and a particular cavity mode, $g_{\rm eff}$, which can be solved by fitting the cavity transmission signal S_{21}:

$$S_{21}(f) = \frac{\kappa_c}{\left(\kappa_c + \frac{\gamma_d}{2}\right) - i(f - f_0) + \frac{g_{\rm eff}^2}{\frac{\gamma_s}{2} - i(f - f_s)}}, \tag{2}$$

where f is the input microwave frequency; f_0 is the frequency of the cavity mode; f_s is the frequency of the spin transition, which is a function of the applied DC magnetic field; κ_c is the coupling of probes to the cavity mode; γ_d is the dielectric loss of the cavity mode; and γ_s is spin loss. One may determine $g_{\rm eff}$ by fitting the maximum of a transmission curve while scanning magnetic field and signal frequency before and after the LZ-assisted thermalisation, or investigate the population dynamics by driving the system on the cavity resonance tuned on the $|+7/2\rangle$ to $\alpha|-3/2\rangle + \beta|+5/2\rangle$ level splitting in the cavity-driven thermalisation approach. By fitting the dependence of the resonance frequencies of S_{21} on the external field, one effective coupling parameter is derived based on many measured data points, covering all significant figures that are given in the results.

3.1. Landau–Zener assisted thermalisation

WGH_{311} (9.45 GHz) and WGH_{211} (7.46 GHz) are selected to couple to spin transition $|-7/2\rangle \rightarrow |-5/2\rangle$ (Probe 1) and $|+7/2\rangle \rightarrow |+5/2\rangle$ (Probe 2) at 26 and 43 mT, respectively (see figure 3). Thus, Probes 1 and 2 give information on the occupancy of levels $|-7/2\rangle$ and $|+7/2\rangle$ respectively via estimated effective couplings $g_{|\pm 7/2\rangle}$ as just stated. In order to observe the LZ-assisted thermalisation, these quantities are measured before (increasing the magnetic field) and after (decreasing the field) tuning the spin ensemble through the avoided level crossing between $|+7/2\rangle$ and $|-5/2\rangle$ levels up to 100 mT. The magnetic field tuning speed is set to 2 mT/min, which is slow enough to ensure completeness of all transients and to avoid any heating effects. The probing field is either kept minimal (much less than the number of impurity ions) or switched on only for the fields when the spin ensemble is tuned on the cavity resonance, so as to avoid any confusion with pumping effects. As a result, we obtain four values of the coupling strengths: $g^{\uparrow}_{|\pm 7/2\rangle}$ for the ensemble–cavity interaction before the LZ transition and $g^{\downarrow}_{|\pm 7/2\rangle}$ after the LZ-assisted relaxation. This allows us to estimate corresponding level occupancies before $N^{\uparrow}_{|\pm 7/2\rangle}$ and after $N^{\downarrow}_{|\pm 7/2\rangle}$. Both numbers must add up to the total number of impurity spins N, as only these levels could be occupied at the temperature of 20 mK:

$$\begin{aligned} N^{\downarrow}_{|+7/2\rangle} + N^{\downarrow}_{|-7/2\rangle} &= N, \\ N^{\uparrow}_{|+7/2\rangle} + N^{\uparrow}_{|-7/2\rangle} &= N. \end{aligned} \tag{3}$$

This relation is experimentally confirmed by the fact that no interactions between the Gd^{3+} ensemble and the microwave modes are observed in the cases when energy levels above $|+7/2\rangle$ play the role of the interaction lower-energy state.

The result of the discussed measurement procedure in terms of the cavity transmission is shown in figure 5. Plots (a) and (b) demonstrate complete leakage of the population from $|+7/2\rangle$ after tuning the system through the level interaction point. We see that the corresponding ALC totally disappears and the corresponding coupling switches from $g^{\uparrow}_{|+7/2\rangle} = 2$ MHz to $g^{\downarrow}_{|+7/2\rangle} = 0$ MHz. On the other hand, density plots (c) and (d) confirm some increase in the ensemble–photon coupling from $g^{\uparrow}_{|-7/2\rangle} = 2.6$ MHz to $g^{\downarrow}_{|-7/2\rangle} = 3.7$ MHz (i.e., by a factor of $\sqrt{2}$), and thus the increase of the population on the ground state by a factor of 2. In terms of the occupancy, the following expected relations are fulfilled:

$$\begin{aligned} 2N^{\uparrow}_{|-7/2\rangle} &= N^{\downarrow}_{|-7/2\rangle}, \\ N^{\downarrow}_{|+7/2\rangle} &= 0. \end{aligned} \tag{4}$$

It should be mentioned that the higher-order mode WGH_{311} is more confined inside the crystal, making coupling strength $g_{|-7/2\rangle}$ larger than $g_{|+7/2\rangle}$ even though $N_{|+7/2\rangle} = N_{|-7/2\rangle}$.

The concentration of Gd^{3+} ion impurities in the crystal can be estimated using coupling strength $g^{\downarrow}_{|+7/2\rangle}$:

$$n = \frac{N^{\downarrow}_{|-7/2\rangle}}{V} = \frac{g^{\downarrow 2}_{|-7/2\rangle}}{g_0^2 V} = 2.5 \times 10^{16}\ \mathrm{cm}^{-3}, \tag{5}$$

where V is the crystal volume and g_0 is estimated using equation (1). This value is small enough to ignore direct spin–spin interaction between Gd^{3+} ions, thus ensuring the phase of the ensemble is paramagnetic [33].

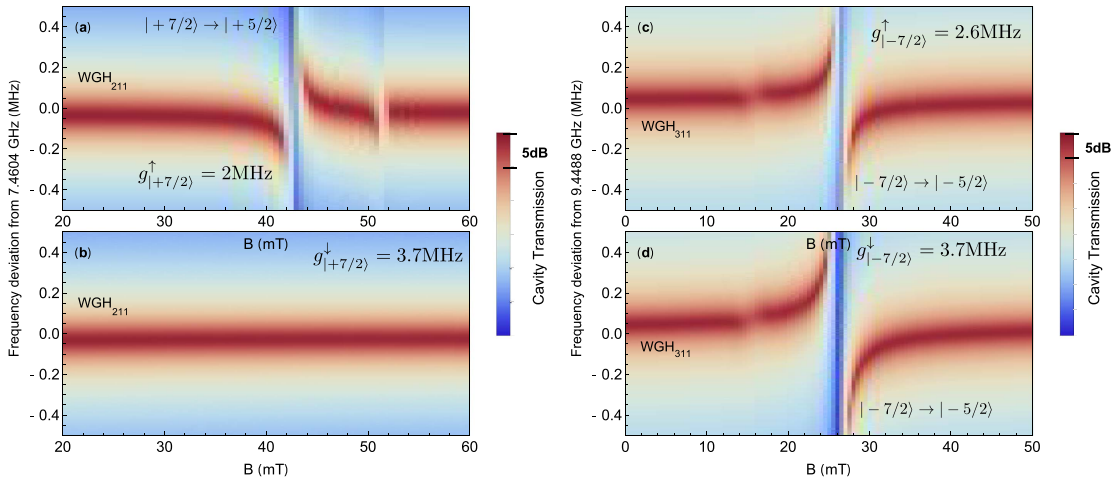

Figure 5. Interaction between WGMs and Gd^{3+}: (a) WGH_{211} and $|+7/2\rangle \rightarrow |+5/2\rangle$ spin transition before LZ transition, (b) WGH_{211} and $|+7/2\rangle \rightarrow |+5/2\rangle$ after LZ transition, (c) WGH_{311} and $|-7/2\rangle \rightarrow |-5/2\rangle$ before LZ transition, (d) WGH_{311} and $|-7/2\rangle \rightarrow |-5/2\rangle$ after LZ transition.

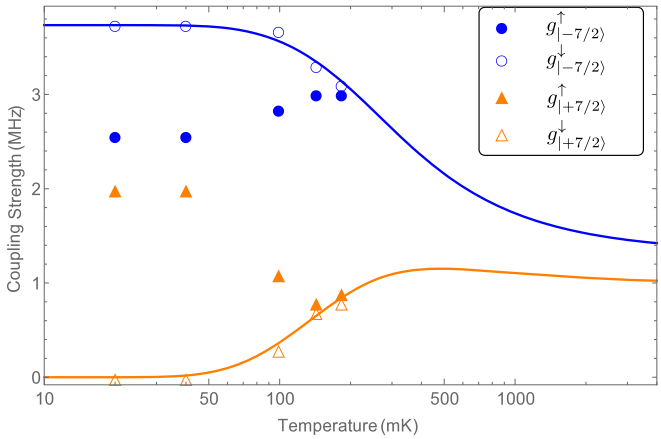

Figure 6. Ensemble-cavity mode coupling strengths $g^{\uparrow}_{|\pm 7/2\rangle}$ and $g^{\downarrow}_{|\pm 7/2\rangle}$ as a function of temperature. The solid curves show predicted values for the system in thermal equilibrium state.

$g^{\uparrow}_{|\pm 7/2\rangle}$ and $g^{\downarrow}_{|\pm 7/2\rangle}$ are further measured as a function of temperature up to 200 mK. The result is shown in figure 6 together with the calculated values for the case of thermal equilibrium (solid curves). The estimations are made assuming the spin energy level structure shown in figure 1 is constant for all temperatures. These results confirm two predictions made previously. First, measured coupling rates $g^{\downarrow}_{|\pm 7/2\rangle}$ at all temperatures are consistent with those calculated in the case of thermal equilibrium, suggesting that the ion ensemble after the LZ transition is in the thermal equilibrium state. Second, measured $g^{\uparrow}_{|\pm 7/2\rangle}$ below 200 mK are distinct from the thermal equilibrium state, suggesting that the thermalisation process between $|\pm 7/2\rangle$ is negligible as described in the previous section. Moreover, when the temperature is below 50 mK, these results correspond to the ensemble distribution shown in equation (3) . Further theoretical investigation of the dynamics for the spin system presented in this work may be performed using approaches used to study Landau–Zener transitions of a single TLS in a dissipative environment [34, 35].

3.2. Cavity-driven thermalisation

Electron spin resonance spectroscopy using WGMs [32] of the YVO_4 crystal at 20 mK revealed the structure of the level interaction of Gd^{3+} ions. The result is shown in figure 7, where both transitions $|+7/2\rangle \rightarrow |+5/2\rangle$ and $|+7/2\rangle \rightarrow |-3/2\rangle$ are observed. Five-photon transition $|+7/2\rangle \rightarrow |-3/2\rangle$ becomes visible due to the final state hybridisation $|+5/2\rangle$, allowing a single-photon transition. The coupling strength between $|+5/2\rangle$ and $|-3/2\rangle$ is estimated to be 220 MHz, giving 5% mixture of $|-3/2\rangle$ with $|+5/2\rangle$ at 43 mT. The solid curves in figure 7 show the estimated spin transitions from the spin Hamiltonian with the 220 MHz level coupling.

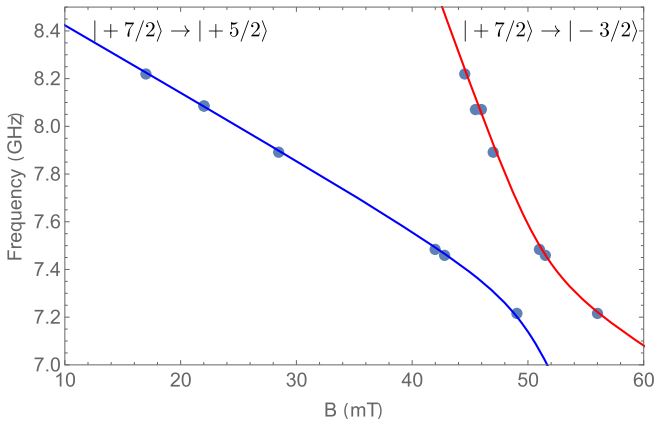

Figure 7. Interaction of spin transitions from $|+7/2\rangle$ to the hybridised states $|+5/2\rangle$ and $|-3/2\rangle$. The solid curves are the calculated transition frequencies.

As described in the previous section, the cavity-driven thermalisation may be observed by tuning the hybridised spin transition onto the WGH_{211} mode and pumping at the cavity resonance. The measured transmission in this case is found from equation (2) by putting $f = f_0 = f_s$ and $g_{\text{eff}} = g_0\sqrt{N^{\uparrow}_{|+7/2\rangle}}$:

$$S_{21}(f_0) = \frac{\kappa_c}{\kappa_c + \gamma_d + \frac{2g_0^2}{\gamma_s}N^{\uparrow}_{|+7/2\rangle}}, \tag{6}$$

where κ_c, γ_d, g_0, and γ_s are constants, giving a dependence of the observed quantity on the occupation of the first excited level.

Time dependence of transmission in equation (6) is measured at 43 mT for different values of the incident power P_{inc}, giving different number of stored photons N_{cav}. The measured transmission is converted into population $N^{\uparrow}_{|+7/2\rangle}$ and shown in figure 8. The result suggests that the population of the $|+7/2\rangle$ level decays to zero, thus approaching thermal equilibrium as described in the previous section. Each observed decay may be separated into two exponential processes giving three time parameters: time constant of the initial decay τ_i, time constant of the finial decay τ_f, transition time from one into the other $T^{\star}$. It is observed that τ_i increases with decreasing power.

To explain these results, the energy level diagram may be approximately reduced to the well-known Λ-scheme with levels $|1\rangle = |+7/2\rangle$, $|2\rangle = \alpha|-3/2\rangle + \beta|+5/2\rangle$, and $|3\rangle = |-7/2\rangle$ (see figure 4). With $\mathbf{N}$ being the vector of populations of corresponding levels, the system dynamics might be described by the following set of ordinary differential equations:

$$\dot{\mathbf{N}} = \begin{pmatrix} -W(N_{\text{cav}}) & \Gamma_{21} & 0 \\ W(N_{\text{cav}}) & -\Gamma_{21} - \Gamma_{23} & 0 \\ 0 & \Gamma_{23} & 0 \end{pmatrix}\mathbf{N}, \tag{7}$$

where $W(N_{\text{cav}})$, Γ_{21}, and Γ_{23} are time constants associated with the cavity pump from $|1\rangle$ to $|2\rangle$ and decay from $|2\rangle$ to $|3\rangle$ and $|1\rangle$. In the limit of strong pumping ($W \gg \Gamma_{31}$ and $W \gg \Gamma_{23}$), two eigenvalues that can be observed through the population of $|1\rangle$ are estimated as $-\frac{1}{2}(\Gamma_{21} + \Gamma_{23})$ and W. These values are estimations of the attenuation rates corresponding to τ_f and τ_i time constants correspondingly observed in the experiment. This result predicts a small power-dependent time constant (slow decay) and a large, almost power-independent time constant (fast decay) that matches the experimental observations in figure 8.

4. Discussion

The unconventional level structure of Gd^{3+} ions in YVO_4 crystal, with the two lowest energy levels split by a seven-photon transition, provides a qubit system with virtually *unlimited relaxation time*. Indeed, truncating the structure between $|+7/2\rangle$ and $|-5/2\rangle$ levels, one comes up with a qubit whose most general state may be written as

$$|\phi\rangle = \alpha|-7/2\rangle + \beta|+7/2\rangle, \tag{8}$$

where $\alpha, \beta \in \mathbb{C}$ and $|-7/2\rangle$ is the ground state. Moreover, at readily accessible temperature of around 20 mK and some external magnetic field, the energy splittings are such that only the ground state is populated at thermal equilibrium. And finally, the energy splitting of such a qubit is externally controllable by the magnetic field. Such

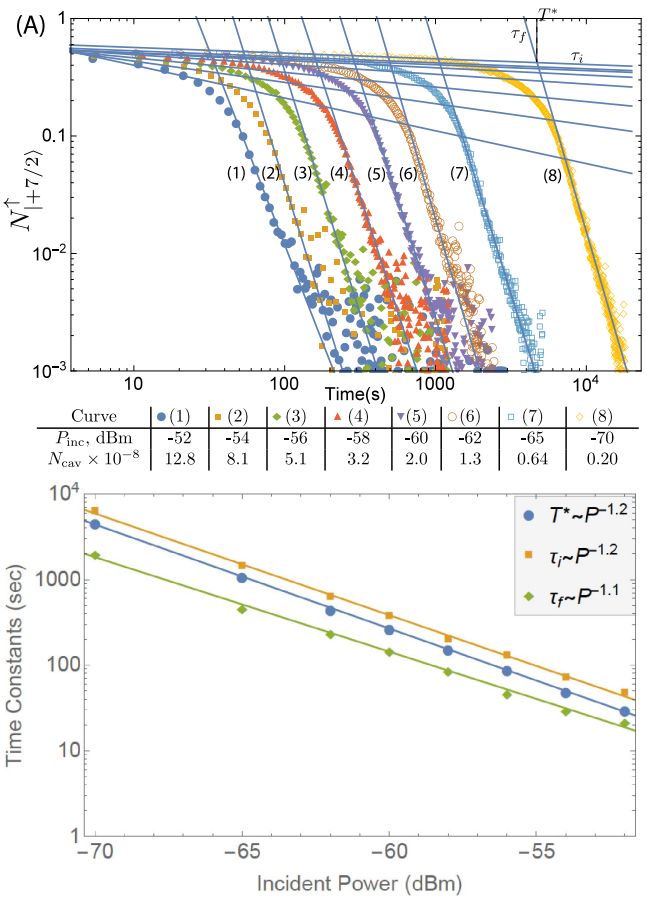

Figure 8. (a) Decay of population of $|+7/2\rangle$ state for continuously pumped cavity for different values of the incident power (see figure 4). (b) Dependence of the time constants of the decay processes on the incident power.

properties could be extremely fruitful for implementation of quantum memories at microwave frequencies that nowadays suffer from relatively low coherence times. Despite the fact that a Gd^{3+}:YVO_4 memory provides unlimited relaxation times, its coherence times should still be experimentally determined. Additionally, such a system cannot be efficiently addressed directly, as it would require some complicated protocols involving higher energy levels and, probably, manipulations with the DC external field.

Also, Landau–Zener–Stückelberg interferometry, based on periodic passage of an avoided level crossing responsible for the LZ transition, has been found to be a useful tool for studying properties of atomic and superconducting qubit systems [36], including perfect population transfer and implementation quantum gates for quantum control and quantum computing [37–39].

Another potential area of application for the considered system is microwave-to-optical quantum converters [6, 7] required for coherent information exchange between local quantum processors. In addition to the advantages of Gd^{3+}:YVO_4 described previously, the very existence of large zero-field splitting is advantageous for such applications since such a hybrid system would not require a large external magnetic field that can negatively influence superconducting parts. Moreover, excellent optical properties of 'vanadate lasers' (rare earth ion-doped YVO_4 and $GdVO_4$) are widely exploited nowadays, mostly in the form of Nd^{3+}:YVO_4 [40, 41] although optical transitions of Gd^{3+} ions in vanadates have to be studied separately.

The quantum level structure of Gd^{3+} in YVO_4 at the zero field is suitable for physical realisation of a continuous-wave maser using an approach similar to that of Fe^{3+} ions in sapphire [3]. Indeed, at zero field, the lower six levels are degenerate in three pairs and form the three-level system $|\pm 7/2\rangle$, $|\pm 5/2\rangle$, $|\pm 3/2\rangle$. By externally pumping the upper level $|\pm 3/2\rangle$ from the ground state $|\pm 7/2\rangle$, one can induce the maser signal associated with one of the decaying processes. Such a maser can be built based on the employed WGM approach by designing the cavity with a resonant mode corresponding to one of the decay processes. A maser system can be also realised at nonzero external magnetic field using, for example, a scheme similar to that in figure 4 and thus exploiting the coupling between energy levels. In this case, the resonator will also be required to have a mode at a desired frequency. In both cases, concentration of Gadolinium ions in the resonator mast be increased.

Another possible application of the Gd^{3+}:YVO_4 system exhibiting the spin angular momentum limitations on some transitions is in microwave detectors that potentially can reach quantum sensitivities. For such a device, highly required for many quantum optics experiments at microwave frequencies, a Λ scheme has been proposed [42, 43]. Such a scheme requires long-lived ground and first excited states together with a short-lived second excited state. These requirements are fulfilled within the cavity-assisted thermalisation scheme depicted in figure 4. Here, the long-lived first excited state $|+7/2\rangle$ is the so-called initial state. By absorbing an external photon, the system transitions into the exited state $\alpha|-3/2\rangle + \beta|+5/2\rangle$, from which it decays into the lowest energy state $|-7/2\rangle$. By monitoring population of this level (or equally $|+7/2\rangle$) with some external macroscpoic parameter depending on the population of these levels, one can count the number of incoming photons. In principle, the cavity-assisted thermalisation experiment demonstrated in this work may be reinterpreted in this way. Here, the role of the external macroscopic parameters is played by the cavity transmission and ensemble spin–photon coupling, although the demonstrated realisation is not in the desired single-photon regime. In order to achieve such a regime, one would have to reduce the cavity linewidth or use some other macroscopic parameters.

In summary, using Gd^{3+}-doped YVO_4 crystal, we demonstrate peculiarities of QED based on a 7/2 spin system with the ground and first excited states separated by a seven-photon transition. In particular it is demonstrated that, by sweeping the external magnetic field from zero, one may generate a nonequilibrium state of the spin ensemble with extremely long lifetimes due to the large number of photons required for the transition between the ground and first excited states. Then it is shown that the equilibrium state may be achieved through the Landau–Zener transition or external cavity drive, made possible due to coupling between excited energy levels. The experiments signify the importance of a particular realisation of a spin ensemble for quantum electrodynamics.

Acknowledgments

This work was supported by the Australian Research Council through grant number CE110001013.

References

[1] Denker B and Shklovsky E 2013 *Handbook of Solid-State Lasers* (Cambridge: Woodhead)
[2] Bourgeois P Y, Bazin N, Kersalé Y, Giordano V, Tobar M E and Oxborrow M 2005 *Appl. Phys. Lett.* **87** 224104
[3] Creedon D L, Benmessai K, Tobar M E, Hartnett J G, Bourgeois P Y, Kersale Y, Floch J M L and Giordano V 2010 *IEEE Trans. Ultrason. Ferroelectr. Freq. Control* **57** 641–6
[4] Pla J J, Tan K Y, Dehollain J P, Lim W H, Morton J J L, Jamieson D N, Dzurak A S and Morello A 2012 *Nature* **489** 541–5
[5] Bertaina S, Gambarelli S, Tkachuk A, Kurkin I N, Malkin B, Stepanov A and Barbara B 2007 *Nat. Nanotechnol.* **2** 39–42
[6] O'Brien C, Lauk N, Blum S, Morigi G and Fleischhauer M 2014 *Phys. Rev. Lett.* **113** 063603
[7] Williamson L A, Chen Y H and Longdell J J 2014 *Phys. Rev. Lett.* **113** 203601
[8] Nicholson T L *et al* 2015 *Nat. Commun.* **6** 6896 EP
[9] Rogge S and Sellars M J 2013 *Nat. Nanotechnol.* **8** 544–5
[10] Maze J R *et al* 2008 *Nature* **455** 644–7
[11] Bluhm R and Kostelecký V A 2000 *Phys. Rev. Lett.* **84** 1381–4
[12] Van Tilburg K, Leefer N, Bougas L and Budker D 2015 *Phys. Rev. Lett.* **115** 011802
[13] Probst S, Rotzinger H, Wünsch S, Jung P, Jerger M, Siegel M, Ustinov A V and Bushev P A 2013 *Phys. Rev. Lett.* **110** 157001
[14] Tkalčec A, Probst S, Rieger D, Rotzinger H, Wünsch S, Kukharchyk N, Wieck A D, Siegel M, Ustinov A V and Bushev P 2014 *Phys. Rev.* B **90** 075112
[15] Hastings-Simon S R, Lauritzen B, Staudt M U, van Mechelen J L M, Simon C, de Riedmatten H, Afzelius M and Gisin N 2008 *Phys. Rev.* B **78** 085410
[16] Goryachev M, Farr W G, Creedon D L and Tobar M E 2014 *Phys. Rev.* A **89** 013810
[17] Goryachev M, Farr W G, Creedon D L and Tobar M E 2014 *Phys. Rev.* B **89** 224407
[18] Verdú J, Zoubi H, Koller C, Majer J, Ritsch H and Schmiedmayer J 2009 *Phys. Rev. Lett.* **103** 043603
[19] Amsüss R *et al* 2011 *Phys. Rev. Lett.* **107** 060502
[20] Lukin M D 2003 *Rev. Mod. Phys.* **75** 457–72
[21] Wisby I S, de Graaf S E, Gwilliam R, Adamyan A, Kubatkin S E, Meeson P J, Tzalenchuk A Y and Lindström T 2016 *Phys. Rev. Applied* **6** 024021
[22] Wang X, Loa I, Syassen K, Hanfland M and Ferrand B 2004 *Phys. Rev.* B **70** 064109
[23] Rosenthal J, Riley R F and Ranon U 1969 *Phys. Rev.* **177** 625–8
[24] Urban W 1968 *J. Chem. Phys.* **49** 2703–5
[25] Kahle H G, Koch V, Plamper J and Urban W 1968 *J. Chem. Phys.* **49** 2702–3
[26] Goryachev M, Farr W G, do Carmo Carvalho N, Creedon D L, Le Floch J M, Probst S, Bushev P and Tobar M E 2015 *Appl. Phys. Lett.* **106** 232401
[27] Probst S, Tkalčec A, Rotzinger H, Rieger D, Le Floch J M, Goryachev M, Tobar M E, Ustinov A V and Bushev P A 2014 *Phys. Rev.* B **90** 100404
[28] Landau L 1932 *Physikalische Zeitschrift der Sowjetunion* **2** 46–51
[29] Zener C 1932 *Proc. R. Soc. Lond. A: Math. Phys. Eng. Sci.* **137** 696–702
[30] Kubo Y *et al* 2010 *Phys. Rev. Lett.* **105** 140502
[31] Schuster D I *et al* 2010 *Phys. Rev. Lett.* **105** 140501

[32] Farr W G, Creedon D L, Goryachev M, Benmessai K and Tobar M E 2013 *Phys. Rev.* B **88** 224426
[33] Farr W G, Goryachev M, le Floch J M, Bushev P and Tobar M E 2015 *Appl. Phys. Lett.* **107** 122401
[34] Nalbach P and Thorwart M 2009 *Phys. Rev. Lett.* **103** 220401
[35] Nalbach P and Thorwart M 2010 *Chem. Phys.* **375** 234–42
[36] Shevchenko S N, Ashhab S and Nori F 2010 *Phys. Rep.* **492** 1–30
[37] Teranishi Y and Nakamura H 1998 *Phys. Rev. Lett.* **81** 2032–5
[38] Gaitan F 2003 *Phys. Rev.* A **68** 052314
[39] Nagaya K, Zhu C and Lin S H 2007 *J. Chem. Phys.* **127** 094304
[40] Connor J R 1966 *Appl. Phys. Lett.* **9** 407–9
[41] Pavel N, Kränkel C, Peters R, Petermann K and Huber G 2008 *Appl. Phys.* B **91** 415
[42] Lanzagorta M 2011 *Quantum Radar Synthesis Lectures on Quantum Computing* (San Rafael,CA: Morgan & Claypool)
[43] Inomata K, Lin Z, Koshino K, Oliver W D, Tsai J S, Yamamoto T and Nakamura Y 2016 *Nat. Commun.* **7** 12303 EP